Image-Based Texture Analysis for Realistic Image Synthesis

HEINZ MAYER[1]

[1]Computer Graphics and Vision, Graz University of Technology
Inffeldgasse 16/II, A-8010 Graz, Austria
mayer@icg.tu-graz.ac.at

Abstract. We present a method to measure reflectance and texture of surfaces in a one step process. For later use in digital image synthesis it is mandatory to separate the gathered intensity values into these two parts to eliminate highlighting artifacts from textures. Our image-based measurement system delivers bidirectional reflectance distribution function (BRDF) values distributed over the surface of the material under investigation. After fitting a reflectance model to the gathered data we estimate the modulation of the diffuse reflectance coefficient which represents the texture. The last step analyzes the texture to get a parameterized and compact description of the measured surface properties. These results allow us to apply the gathered surface properties to objects with arbitrary shape and size. To keep the measurement system simple a standard CCD camera and light source are used.
Keywords. Texture analysis, surface properties, BRDF, rendering, physically-based

1 Introduction

Physically-based lighting simulation needs an accurate global illumination algorithm and a geometric description of the scene as well as physically-based descriptions of the light sources and material properties [9]. Since implementations of rendering algorithms for lighting calculations are available such as the RADIANCE system [21] and physically-based parameters are available for a number of light sources too we concentrate our work on measuring parameters out of real-world surfaces.

One approach to estimate material parameters would be to use a photogoniometer and take a large number of BRDF measurement points well distributed over the incoming and outgoing radiation hemisphere. Afterwards an appropriate reflectance model can be fitted to this point-cloud. The disadvantages of this method are the time and cost intensive way of gathering BRDF values and the fact that we have no information about the parameter distribution over a certain region of the probe. This means that we will get correct model parameters for only one surface point. To extend that method for texture estimation we have to apply this procedure to a lot of surface points of the material under investigation, which makes this method even more time and cost expensive.

Since we like to have a whole library of different materials, which we can use for lighting simulation, we started to implement an image-based method to measure anisotropic reflection. The system works on digital images acquired from real surfaces and reconstructs BRDF values. Furthermore the equipment used should be cheap and measurement time should be reasonable. More details of the structure is given in Section 3. The measured BRDF values are then used to estimate the modulation of the diffuse reflectance coefficient which represents the texture. This is possible in cause of BRDF values are distributed over the surface of the material and are not taken only from one surface point. No preliminary knowledge of the material or equipment is necessary only some geometric constraints as described in Section 3 has to be fulfilled.

2 Background and Previous Work

In graphics a light–material interaction is usually defined by the term bidirectional reflectance distribution function ($f_r, [\mathrm{sr}^{-1}]$). This function can be physically expressed as ratio of reflected radiance in a given direction (θ_r, ϕ_r) to the incident irradiance enter the surface from the direction (θ_i, ϕ_i). Geometrical considerations and nomenclature can be found in [17].

$$\begin{aligned} f_r(\lambda, \theta_r, \phi_r, \theta_i, \phi_i) &= \frac{dL_{\lambda,r}(\lambda, \theta_r, \phi_r, \theta_i, \phi_i)}{dE_{\lambda,i}(\lambda, \theta_i, \phi_i)} \\ f_{r,ideal} &= 1/\pi \\ f_{r,standard} &= \frac{\rho_{standard}}{\pi} \end{aligned}$$

For perfect diffuse surfaces f_r is independent from the variables $\theta_r, \phi_r, \theta_i, \phi_i$. Especially for the ideal standard surface the BRDF can be defined as $f_{r,ideal}$. The reference material ($f_{r,standard}$) used has a reflectance coefficient ($\rho_{standard}$) which is nearby constant (approx. 0.99) over the whole visual spektrum. Detailed product specifications can be found in [4].

Considerable previous work has been done on image-based measurement of material properties. Methods for anisotropic reflectance without texture are introduced in [20].

0-7695-0878-2/00 $10.00 © 2000 IEEE

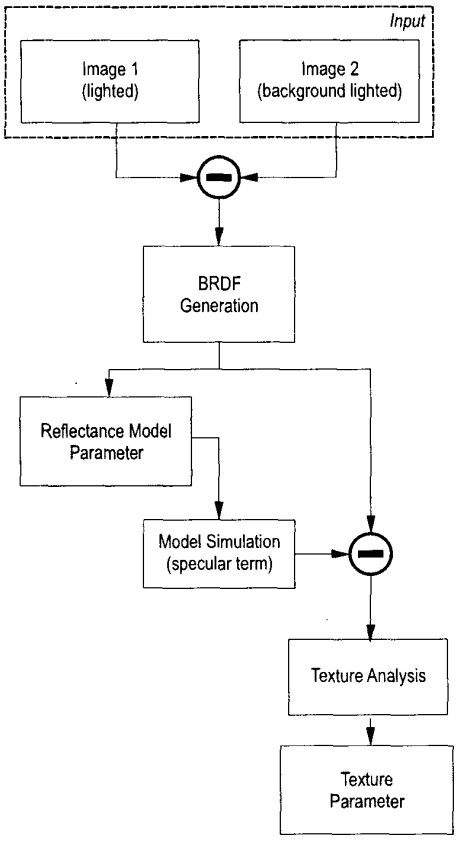

Figure 1: Overview of the method.

In [15] a BRDF measurement method of surfaces even for the human skin is presented. A complex image acquisition system including a camera, range finder, and a robotic arm is used in [19] to reconstruct the geometry of the object first and estimate the diffuse and specular reflectance afterwards. The measurement system used in [5] also uses a robotic arm to position and orient the samples in relation to a light source and camera. Texture information of one sample is stored in a number of images whereas different viewing and illumination orientations are used. Therefore the rendering process can utilize view-dependent texture mapping which gives the impression of bump mapping. Recent interesting work has also been done on recovering reflectance characteristics using images taken from indoor and outdoor scenes by exploiting inverse rendering techniques [22], [23], [14].

3 BRDF Measurement System

An overview of the concept for recovering reflectance model parameters and texture parameters is given in Figure 1. Before we describe how to obtain the parameters in detail we give an explanation of BRDF reconstruction.

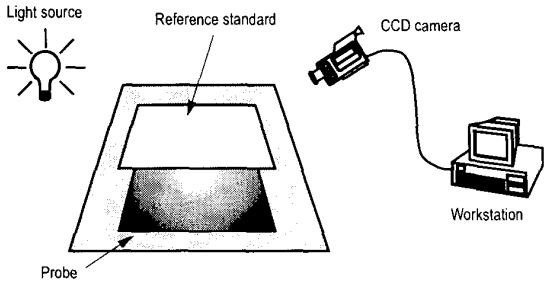

Figure 2: Structure of the measurement system.

Figure 2 shows the geometric configuration of light source, camera, the reference standard, and the probe. One restriction is that light source, camera, and stripline between probe and reference standard must lie in one plane and this plane must be orthogonal to the measurement plane. This restriction is necessary to reconstruct the corresponding BRDF values of the probe with the image intensities gathered. To let this reconstruction work a symmetric distribution of light source radiation is necessary.

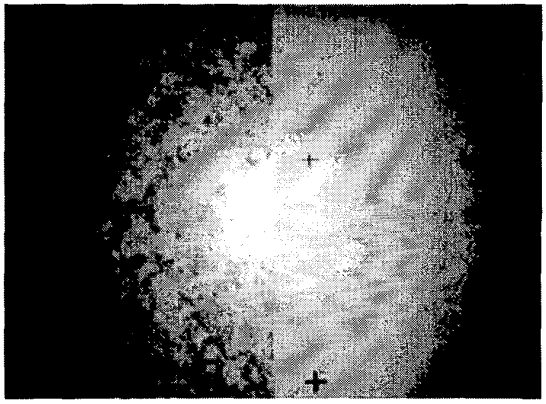

Figure 3: Image taken by a standard CCD camera showing the probe (desk) on the left side and reference standard on the right.

Since no additional housing is used to protect the probe from background lighting two images were taken by the camera. One with the light source turned off and the other one with the light source turned on. The BRDF values can then be reconstructed by the following relation:

$$f_{r,measured} = \frac{v_{measured} - v_{background_1}}{v_{standard} - v_{background_2}} \cdot \frac{\rho_{standard}}{\pi}$$

where:

$v_{measured}$	the measured radiance value at the location of interest,
$v_{standard}$	the measured radiance value at the symmetric location of the diffuse reflectance standard,
$v_{background_1}$	the background radiance of the location of interest,
$v_{background_2}$	the background radiance of the symmetric location of the diffuse reflectance standard

After recovering absolute BRDF values fitting of the model parameters is carried out by a least-squares method [13] with a reasonable number of points. We use the Ward reflectance model [20] because it is computationally inexpensive and can be applied to a number of different materials. A more detailed description of the structure and the image-based BRDF measurement for anisotropic reflection can be found in [11]. The geometrical considerations for the input variables are shown in Figure 4.

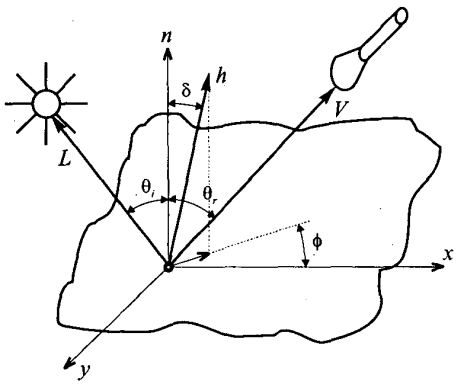

Figure 4: Geometry of input variables for BRDF parameter reconstruction.

The model consists of a diffuse and a specular term, which can be either isotropic or anisotropic:

$$f_{r,Ward} = \frac{\rho_d}{\pi} + \frac{\rho_s}{\sqrt{\cos\theta_i \cos\theta_r}} \cdot K$$

K for isotropic reflectance:

$$K = \frac{\exp\left[-\tan^2\delta/\alpha^2\right]}{4\pi\alpha^2}$$

where:

θ_i	incident polar angle
θ_r	polar angle related to the camera
δ	angle between vectors $\vec{n}$ and $\vec{h}$ shown in Figure 4
ρ_d	diffuse reflectance
ρ_s	specular reflectance
α	standard deviation of the surface slope

And for the anisotropic case where specular reflectance depends on the orientation of the probe the parameter α splits into two parameters α_x and α_y as well as the additional variable ϕ is necessary.

$$K = \frac{\exp\left[-\tan^2\delta(\cos^2\phi/\alpha_x^2 + \sin^2\phi/\alpha_y^2)\right]}{4\pi\alpha_x\alpha_y}$$

The wavelength dependence is eliminated for convenience. Due to our imaging device we use the RGB triple for representing color. Figures 5 and 6 show examples of measured BRDF values of one vertical image scanline and the corresponding reconstructed BRDF characteristics. Because there is no texture information included in the calculated values this curve is much smoother than the original measured data.

Since specular reflectance is mostly a global material characteristic we take the assumption that the model parameters for the specular term $(\rho_s, \alpha_x, \alpha_y)$ do not change for the whole surface. On the other hand this means that the local variation of the measured BRDF values can be expressed as variation of the diffuse reflectance coefficient ρ_d. The next section gives a complete explanation on how to separate specular reflectance and the texture information.

4 Texture Analysis and Synthesis

4.1 Image Textures

One of the advantages of our measurement method is that we have knowledge about the BRDF value distribution over the surface. For the reflectance model used the diffuse and specular reflectance terms can easily be separated. Therefore we estimate these parameters using a least-squares solution, as in [11], and can extract the texture of the surface out of an image without specular artifacts.

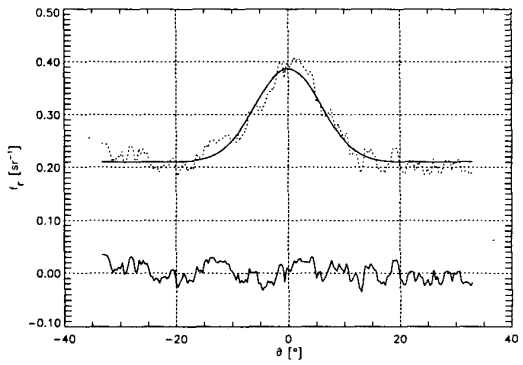

Figure 5: Desk BRDF characteristics (see Figure 3 for reference).

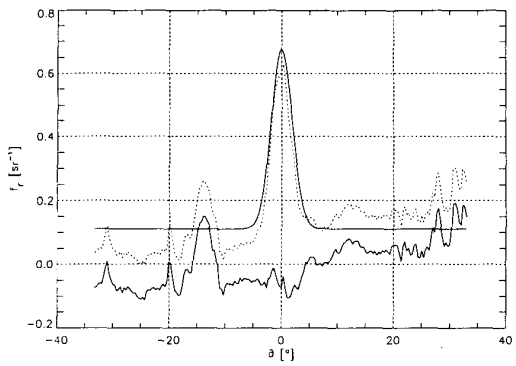

Figure 6: Marble BRDF characteristics.

Each of Figure 5 and 6 shows three curves. To verify the BRDF model fitting one curve shows the measured BRDF values and the second one represents the result of the reconstructed model. Additionally the last curve shows the modulation of ρ_d. The texture information can then be expressed as difference of measured BRDF values and reconstructed specular term:

$$\rho_{d,texture} = \pi(f_{r,measured} - \frac{\rho_s}{\sqrt{\cos\theta_i \cos\theta_r}} \cdot K)$$

Using the convention defined in Section 2 $\rho_{d,texture}$ is defined as the modulation of the total diffuse reflectance. Values given in the diagrams are taken from one vertical scanline nearby the centerline to demonstrate that the separation of diffuse and specular term works even in regions with strong specular highlights.

Figure 7: Image texture with subtracted specular component. Original image can be found in Figure 3.

The results for the whole image are shown in Figure 7. What we can see is that the intensity is uniform almost in every region of the image and most of the radiometric distortions coming from the CCD camera are corrected too. The reddish appearance of the original image is suppressed but in regions with high or low intensities artifacts due to saturation of the camera in one hand and discretization on the other hand still remain. These problems are discussed in detail in Section 5. Furthermore white markers appear in texture regions where their aren't any markers in the original image. The reason is that at these regions no reference data taken from symmetric points on the standard material are available. For the parametric texture analysis described in the following section we leave such regions out.

4.2 Parameterized Textures

It was our aim to measure material properties and to get a compact description which can be reused for objects with arbitrary shape and unlimited spatial extent. For the reflectance model the first and second conditions are fulfilled. The four parameters $\rho_d, \rho_s, \alpha_x, \alpha_y$ describe a wide range of materials even with anisotropic reflectivity and the resulting model does not imply any restriction to surface shape or extent. This is not the case for image textures. Two limitations are inherent in the used representation. One is the geometric resolution which is given by the resolution of the CCD camera and the second is the spatial extent which is also restricted by the camera's field-of-view. Simple tiling would not be a solution for photorealism applications. So we introduce parameterized or so-called procedural textures [7] to our method. This yields to overcome the presented restrictions and additionally leads to a very compact description. Another advantage of using parameter estimation even for the texture is that the artifacts coming from the data acquisition like saturation and discretization effects and also noise can be reduced.

A completely automatic pyramid based approach that requires only a digital image as input is developed by David Heeger et al. [10]. Since this prerequisite fits perfectly our measurement method and the fact that various textures can be analyzed we use this algorithm for the last step in our system. The only important thing we have to reconsider is which filters to use for building the pyramid.

The algorithm introduces two concepts to analyze and synthesize a digital image, image pyramids [3] and histogram matching. We start with a representative region (Figure 9) out of the measured texture (Figure 7). The basic idea behind image pyramids is to extract coefficients out of images for different frequency bands. Thus filtering and resampling processes are used to build up all image pyramid levels. Heeger proposes to use either a Laplacian or a steerable pyramid [18]. The Laplacian pyramid uses a low- and a high-pass filter for frequency analysis and the steerable pyramid additionally

four band-pass filters. This makes the Laplacian pyramid more compact than the other one which can be a critical point for large digital images. In our case we are interested in accurate parameter extraction of digital images of limited size. Therefore we decided to use the steerable pyramid since the orientation information of structures within the texture is better represented in the four band-pass filters. The filters are designed to separate the input signal into four different orientation bands. The cumulative distribution function (CDF) of each of this frequency- and orientation-subbands of all pyramid levels are now the parametric representation of the material texture.

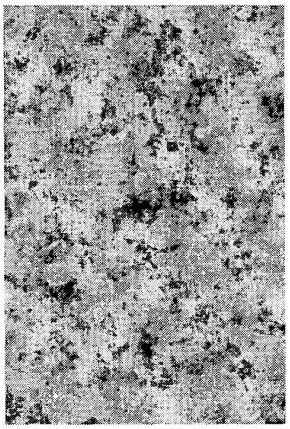

Figure 8: Synthetic image texture, parameters taken from texture analysis of image in Figure 7

Synthesis of textures with arbitrary resolution is carried out by matching the CDF of the subbands in the pyramid levels of an initial noise image with the CDF extracted in the analysis step. We refer this step to histogram-matching. Since this histogram-matching operation does not produce an exact and unique solution several iterations are necessary. Synthetic images (i.e. Figure 8) presented here are generated with three iterations of histogram-matching.

5 Results

The images presented are generated by the use of a 50W quartz lamp, an SGI Indy workstation with additional CCD camera and a reference target (barium sulfate coated). A discussion of the achieved results as well as principle limitations of the method are given in the next two subsections.

5.1 Materials under Investigation

If we roughly categorize the reflectance characteristics of arbitrary materials into the three groups diffuse, specular-diffuse and specular we concentrate our tests on materials with specular-diffuse reflectivity. For materials with near to perfect diffuse reflectivity the problem of measuring and analyzing textures from digital images is reduced to the analysis step since intensity increases through specular highlighting are no longer visible. And for materials with highly specular reflectivity we do have limitations coming from the capabilities of the imaging device (see discussion on limitations in Section 5.2).

To demonstrate the potential of the method a material with lower specular component (desk) and a material with higher specular component (marble) are chosen. The results of the BRDF model fitting is shown in Table 1. Results of the texture analysis and synthesis steps are documented within the next pictures.

Material	ρ_d	ρ_s	α_x	α_y
desk	0.676	0.039	0.137	0.150
marble	0.348	0.013	0.041	0.056

Table 1: BRDF model parameters for materials

5.1.1 Desk

In Figure 5 we can see that the fitting process of measured BRDF values delivers plausible results. We can verify this visually through comparison of measured values (rough curve) with calculated values (smooth curve) shown in the diagram. The BRDF values are generated out of the corresponding input images (see Figure 3). To verify the ability to generate textures with arbitrary aspect ratio and spatial extent a number of synthesized textures with the same input parameters are presented in Figure 10. The parameters are taken from analysis of texture region shown in Figure 9. This also demonstrates the capability to represent seamless textures.

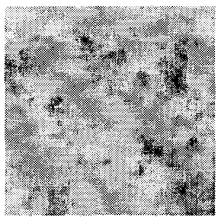

Figure 9: Selected region for texture analysis.

5.1.2 Marble

Due to the higher specularity of the marble probe and the low dynamic range of the used CCD camera more color distortions compared to the desk probe appear in the middle of the image shown in Figure 12. Additionally

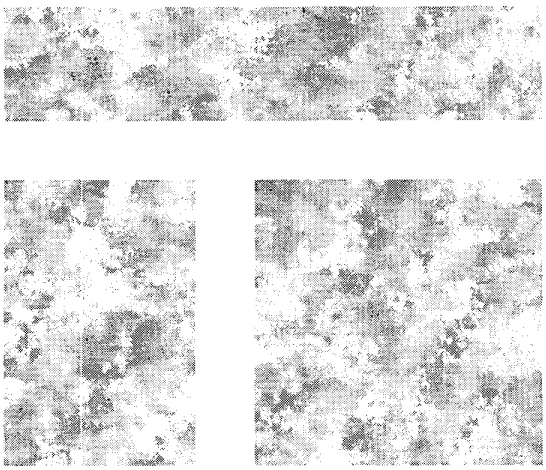

Figure 10: Texture synthesis with different resolution and aspect ratios; parameters taken from analysis of image in Figure 9.

texture information get lost in cause of saturation of the camera. All other regions seem to be equally illuminated as we expect if someone removes the specular reflectivity from a surface. The BRDF model parameter verification again can be realized in Figure 6.

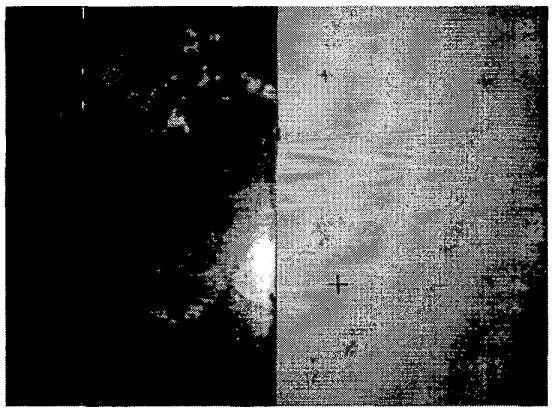

Figure 11: Image taken by a standard CCD camera showing the probe (desk) on the left side and reference standard on the right.

For the analysis and synthesis of a selected region one limitation can slightly be noticed in Figure 13. The image, which is geometrically scaled by a factor of two, seems to be a little bit blurred compared to the input image. This comes from the property of the used steerable pyramid that sharp regular structures are not well represented. The next subsection will discuss this limitation as well as others coming from the imaging device, used reflectance model, and geometric constraints of the BRDF measurement system.

Figure 12: Image texture with subtracted specular component. Original image can be found in Figure 11.

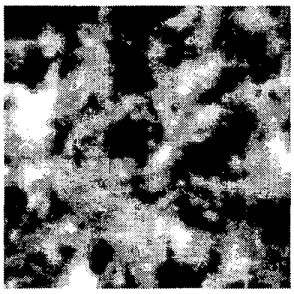

Figure 13: Synthetic image texture, parameters taken from texture analysis of image in Figure 12.

5.2 Limitations

It was our intention to build a measurement system which is not time and cost intensive. These restrictions and properties of the used texture analysis and synthesis led to some limitations inherent in the method which will be explained in detail in the following paragraphs. Some of them could be eliminated as proposed in Section 6.

5.2.1 Specular Reflection

Looking at the equipment the symmetry constraint for the radiation distribution of the light source holds even for our simple quartz lamp.

The second important component, the CCD camera, is the major drawback in the system especially for highly specular materials. This kind of cameras have a limited dynamic range which is based on the physical effect they use for image acquisition. Highly specular and textured materials deliver images with high-intensive spots and

low-intensive textures. An image capturing device with high dynamic range or a software solutions to extend the dynamic range of standard CCD cameras, as introduced in [6] are necessary if we would measure this kind of materials.

Another restriction for measuring highly specular materials comes from the used reflectance model which is not well suited for this case. This limitation can be eliminated since our method allows to exchange the reflectance model with no additional effort. Recent work is published on compact metallic reflectance models in [16].

Additionally there are some materials where not only the diffuse but also the specular reflectance coefficient varies over the surface.

5.2.2 Surface Geometry

We exploit the symmetry of our measurement structure to gather BRDF reference points. At the current state this works only if the material under investigation has a planar surface.

5.2.3 Surface Roughness

We suppose that the variation of the measured BRDF values represent the modulation of the diffuse reflectance coefficient. If we measure materials with a macroscopic surface roughness additional shading and shadowing effects influence the resulting digital image. In this case the extracted texture parameters do not represent the texture of the probe. The result is a mixture of texture, shading, and shadowing effects from surface bumps.

5.2.4 Structured Textures

Figure 14 shows an example of a texture where analysis and synthesis will fail. The synthesized texture in Figure 15 exposes the expected color impression but the regular structures get lost. This comes from the property that the steerable pyramid based algorithm cannot represent regular structures with high frequency content over a wide area.

6 Conclusions and Future Work

We have presented a method to measure material properties out of digital images. The results are reflectance model parameters and parameters for the texture of the surface. We achieve these results by fitting a reflectance model to the measured BRDF values and subtract the simulated specular component from the image texture. The following texture analysis delivers a parametric representation for later use in realistic image synthesis.

The presented examples demonstrate the capabilities of our method. Materials with diffuse up to specular-diffuse characteristics can be modeled with some restrictions. These restrictions are limited specular components for the reflectance model parameter fitting and irregularity and inhomogenity for the texture analysis.

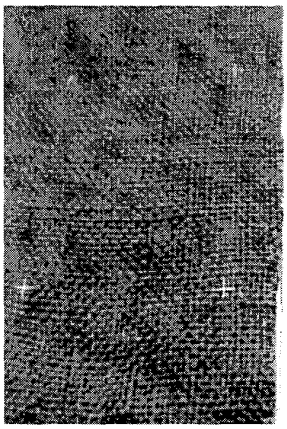

Figure 14: Image texture with subtracted specular component. A typical example where texture analysis/synthesis will fail

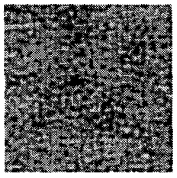

Figure 15: Synthetic image texture, parameters taken from texture analysis of image in Figure 14

Future work will be done to overcome some of the limitations described in Section 5:

- Improvement of the image acquisition process: i.e. employment of modern CMOS cameras with high dynamic ranges ($\approx 10^6$) and integration of techniques presented in [6].
- Implementation of further reflectance models even for metallic materials [16], [12].
- Invent new texture analysis algorithms as introduced in [8] and [2].

References

[1] ACM. *Computer Graphics (SIGGRAPH '97 Proceedings)*, August 1997.

[2] Jeremy S. De Bonet. Multiresolution sampling procedure for analysis and synthesis of texture images. In *Computer Graphics (SIGGRAPH '97 Proceedings)* [1], pages 361–368.

[3] P.J. Burt and E.H. Adleson. The Laplacian pyramid as a compact image code. *IEEE Transactions on Communications*, 31(4):532–540, April 1983.

[4] Munsell Color. White reflectance coating specifications. `http://www.munsell.com/`.

[5] Kristin J. Dana, Bram van Ginneken, Shree K. Nayar, and Jan J. Koenderink. Reflectance and texture of real-world surfaces. *ACM Transactions on Graphics*, 18(1):1–34, Jan 1999.

[6] Paul E. Debevec and Jitendra Malik. Recovering high dynamic range radiance maps from photographs. In *Computer Graphics (SIGGRAPH '97 Proceedings)* [1], pages 369–378.

[7] David S. Ebert, F.Kenton Musgrave, Darwyn Peachey, Ken Perlin, and Steven Worley. *Texturing and Modeling: A procedural Approach*. AP Professional, 2nd. edition, 1998.

[8] Alexei A. Efros and Thomas K. Leung. Texture synthesis by non-parametric sampling. In *IEEE International Conference on Computer Vision*, volume II, pages 1033–1038, Sep 1999.

[9] Donald P. Greenberg et al. A framework for realistic image synthesis. In *Computer Graphics (SIGGRAPH '97 Proceedings)* [1], pages 477–494.

[10] David J. Heeger and James R. Bergen. Pyramid based texture analysis/synthesis. In *Computer Graphics (SIGGRAPH '95 Proceedings)*, volume 29, pages 229–238. ACM, August 1995.

[11] Konrad F. Karner, Heinz Mayer, and Michael Gervautz. An image based measurement system for anisotropic reflection. In *EUROGRAPHICS Annual Conference*, volume 15, pages 119–128. Eurographics Association, August 1996.

[12] Eric P. F. Lafortune, Sing-Choong Foo, Kenneth E. Torrance, and Donald P. Greenberg. Non-linear approximation of reflectance functions. In *Computer Graphics (SIGGRAPH '97 Proceedings)* [1], pages 117–126.

[13] R.L. Launer and G.N. Wilkinson. *Robustness in Statistics*. Academic Press, 1979.

[14] Stephen R. Marschner. *Inverse Rendering in Computer Graphics*. PhD thesis, Program of Computer Graphics, Cornell University, Ithaca, NY, 1998.

[15] Stephen R. Marschner, Stephen Westin, Eric P.F. Lafortune, Kenneth Torrance, and Donald Greenberg. Image-based brdf measurement including human skin. In *EUROGRAPHICS Workshop on Rendering*. Eurographics Association, June 1999.

[16] Laszlo Neumann, Attila Neumann, and Laszlo Szirmay-Kalos. Compact metallic reflectance models. In *EUROGRAPHICS Annual Conference*, volume 18, pages 161–171. Eurographics Association, September 1999.

[17] F. E. Nicodemus, J. C. Richmond, J. J. Hsia, I. W. Ginsberg, and T. Limperis. Geometric considerations and nomenclature for reflectance. Monograph 161, National Bureau of Standards (US), October 1977.

[18] Pietro Perona. Deformable kernels for early vision. *IEEE Transactions on Pattern Analysis and Machine Intelligence*, 17(5):488–499, May 1995.

[19] Yoichi Sato, Mark D. Wheeler, and Katsushi Ikeuchi. Object shape and reflectance modeling from observation. In *Computer Graphics (SIGGRAPH '97 Proceedings)* [1], pages 379–387.

[20] Gregory J. Ward. Measuring and modeling anisotropic reflection. In *Computer Graphics (SIGGRAPH '92 Proceedings)*, volume 26, pages 265–272. ACM, July 1992.

[21] Gregory J. Ward. The RADIANCE lighting simulation and rendering system. In *Computer Graphics (SIGGRAPH '94 Proceedings)*, volume 28, pages 459–472. ACM, July 1994.

[22] Yizhou Yu, Paul Debevec, Jitendra Malik, and Tim Hawkins. Inverse global illumination: Recovering reflectance models of real scenes from photographs. In *Computer Graphics (SIGGRAPH '99 Proceedings)*, pages 215–224. ACM, August 1999.

[23] Yizhou Yu and Jitendra Malik. Recovering photometric properties of architectural scenes from photographs. In *Computer Graphics (SIGGRAPH '98 Proceedings)*, pages 207–218. ACM, July 1998.